The Electrostatic Nature of C3d-Complement Receptor 2 Association[1]

Dimitrios Morikis[2]* and John D. Lambris[†]

The association of complement component C3d with B or T cell complement receptor 2 (CR2 or CD21) is a link between innate and adaptive immunity. It has been recognized in experimental studies that the C3d-CR2 association is pH- and ionic strength-dependent. This led us to perform electrostatic calculations to obtain a theoretical understanding of the mechanism of C3d-CR2 association. We used the crystallographic structures of human free C3d, free CR2 (short consensus repeat (SCR)1–2), and the C3d-CR2(SCR1–2) complex, and continuum solvent representation, to obtain a detailed atomic-level picture of the components of the two molecules that contribute to association. Based on the calculation of electrostatic potentials for the free and bound species and apparent pK_a values for each ionizable residue, we show that C3d-CR2(SCR1–2) recognition is electrostatic in nature and involves not only the association interface, but also the whole molecules. Our results are in qualitative agreement with experimental data that measured the ionic strength and pH dependence of C3d-CR2 association. Also, our results for the native molecules and a number of theoretical mutants of C3d explain experimental mutagenesis studies of amino acid replacements away from the association interface that modulate binding of iC3b with full-length CR2. Finally, we discuss the packing of the two SCR domains. Overall, our data provide global and site-specific explanations of the physical causes that underlie the ionic strength dependence of C3d-CR2 association in a unified model that accounts for all experimental data, some of which were previously thought to be contradictory. *The Journal of Immunology,* **2004, 172: 7537–7547.**

The complement system is part of innate immunity and its regulated activation targets invading foreign pathogens. In pathological situations, unregulated complement activation targets host tissues. Complement activation proceeds through three different pathways, the classic, the lectin, and the alternative, all of which converge through complement component C3. Proteolytic cleavage of C3 produces the anaphylatoxin C3a, a mediator of inflammatory response, and C3b, the opsonin that covalently attaches to foreign pathogens and acts as a tag for subsequent elimination by macrophages. The site of covalent attachment of C3b involves a cysteine that becomes exposed only after proteolytic cleavage or hydrolysis of C3. This site is present in subsequent proteolytic cleavage fragments iC3b, C3dg, and C3d. When C3d is bound to foreign Ags it can simultaneously bind to B cell complement receptor 2 (CR2,[3] also known as CD21). CR2 is part of the B cell coreceptor complex that consists of CD19, CR2, and CD81. The attachment of foreign Ag to CR2 through C3d facilitates the cross-linking of the Ag to membrane-bound Ig to form the B cell Ag-receptor complex together with transmembrane molecules Igα and Igβ. The cross-linking is essential when Ag concentration is low because it amplifies the B cell activation through a signal transduction cascade involving CD19 of the coreceptor complex, tyrosine kinases, and the Igα and Igβ of the receptor complex. This function makes the C3d-CR2 complex a link between innate and adaptive immunity (1–12).

CR2 is also the obligate receptor for the EBV glycoprotein gp350/220 and CD23. CR2 consists of 15 or 16 short consensus repeat (SCR) domains (also known as complement control protein modules), but the first two SCRs are critical for binding to all of its three ligands (13–22). The crystallographic structure of the C3d-CR2(SCR1–2) complex has shown that only one SCR, SCR2, of CR2 is in contact with C3d (19), but it has been proposed that the other SCR, SCR1, participates allosterically in association (22). Earlier studies have shown that both SCR1 and SCR2 are essential and sufficient for C3d-CR2 interaction (13, 14, 16, 18, 20). The first two SCRs of CR2 have also been identified as the sites of association with the EBV glycoprotein gp350/220 (13, 15, 18, 22). Finally, the sites of interaction of CR2 with CD23 were located in SCR5–8 with contribution from SCR1–2 (17). SCR domains have a conserved core and are linked with variable length linkers (23). Several SCR domains can form chains that are not only part of the complement family, such as CR1, CR2, factor H, and the membrane attack complex, but are also noncomplement family proteins, such as the vaccinia control protein, which structurally resembles CR2 but is composed of four SCRs only. It has been proposed that the flexibility and relative orientation of SCR domains, mediated by the variable length interdomain linker, and by the presence (or absence) of side-by-side packing, mediated by hydrophobic side chains, is important for function (19, 22–32).

The nature of C3d-CR2 interaction has been a subject of intense study and speculation, with a variety of experimental data being available. It has been recognized in a number of studies that C3d-CR2 association is pH- and ionic strength-dependent (20, 33–36). Similar pH and ionic strength dependence was also observed in the

*Department of Chemical and Environmental Engineering, University of California, Riverside, CA 92521; and [†]Protein Chemistry Laboratory, Department of Pathology and Laboratory Medicine, School of Medicine, University of Pennsylvania, Philadelphia, PA 19104

Received for publication October 7, 2003. Accepted for publication April 1, 2004.

The costs of publication of this article were defrayed in part by the payment of page charges. This article must therefore be hereby marked *advertisement* in accordance with 18 U.S.C. Section 1734 solely to indicate this fact.

[1] This work was supported by National Institutes of Health Grant AI30040.

[2] Address correspondence and reprint requests to Dr. Dimitrios Morikis, Department of Chemical and Environmental Engineering, University of California, Riverside, CA 92521. E-mail address: dmorikis@engr.ucr.edu

[3] Abbreviations used in this paper: CR, complement receptor; SCR, short consensus repeat; SASA, solvent accessible surface area; NMR, nuclear magnetic resonance; C3d, the d-fragment of complement component C3; CR2(SCR1–2), free CR2 consisting of the first two SCRs; C3d-CR2(SCR1–2), the complex of C3d with the first two SCRs of CR2; CR2(a), the first molecule of CR2(SCR1–2) of structure with PDB code 1ghq; CR2(b), the second molecule of CR2(SCR1–2) of structure with PDB code 1ghq.

 0022-1767/04/$02.00

homologous interaction between C4b and C4-binding protein (37, 38). The three-dimensional structures of free C3d (39), free CR2(SCR1–2) (22), and of the C3d-CR2(SCR1–2) complex (19) are now available and enable us to critically examine the nature of C3d-CR2 association and the conformational changes involved. The structure of free C3d became first available and revealed the presence of an acidic pocket that was thought to be a candidate for the association site with CR2 (39). Subsequent mutagenesis studies within the acidic pocket of C3d in iC3b demonstrated either loss or gain of binding ability to CR2(SCR1–15)-bearing Raji cells and supported this hypothesis (35). However, the structure of the C3d-CR2(SCR1–2) complex became available later, showing that the association site was not at, or close to, the acidic pocket (35). This is a contradictory result to the mutagenesis data within the mindset that residues located at the association interface are solely responsible for association, and if there are no additional association sites. Thus, the mechanism of C3d-CR2 association has been a puzzle up to now.

Given the pH and salt dependence of C3d-CR2 or iC3b-CR2 association (20, 33–36) and the importance for association of specific charges away from the crystallographic association site (35), we have performed electrostatic calculations to predict the pK_a values of all ionizable residues of free C3d, free CR2(SCR1–2), and the C3d-CR2(SCR1–2) complex. Perturbations in pK_a values because of complex formation and sensitivity of pK_a values to ionic strength have provided insight into the nature of C3d-CR2 association. We have also constructed theoretical mutants of C3d in accord with the previously reported experimental mutants that were shown to modulate iC3b-Raji cell CR2(SCR1–15) association (19, 35). We have used the theoretical mutants to calculate electrostatic potentials and to make correlations between them and C3d-CR2 association.

Theoretical electrostatic potential and pK_a calculations are useful tools in understanding the formation of the three-dimensional structure of biomolecules, biomolecular complexes and assemblies (40), and biophysical processes such as folding and stability (41), structural transitions (42) and their stability (43), association (44), ligand binding (45), substrate binding (46), and catalysis (47). The references above are only representative from a large literature pool. Our studies used the solution of the Poisson-Boltzmann equation with finite difference method to calculate electrostatic potentials, based on the available crystallographic structures and continuum solvent representation. We will discuss the effects of the experimentally important ionizable residues for association and we will provide theoretical evidence on the nature of C3d-CR2 association. This discussion involves: 1) residues buried at the association interface that, expectedly, affect binding; 2) ionizable residues away from the association interface that, unexpectedly, affect binding; 3) ionizable residues involved in inter- and intramolecular salt bridges or hydrogen bonds, the latter throughout the volume of C3d, that show ionic strength dependence and participate in modulating the binding of C3d to CR2; 4) the nature of SCR1/SCR2 packing in CR2 that mediates specificity for binding to C3d through a network of hydrophobic and polar interactions. Our discussion will critically examine previously proposed models and hypotheses for C3d-CR2 association and SCR1/SCR2 packing (19, 22, 35, 39).

Materials and Methods

The calculation of apparent pK_as of ionizable sites in the interior of proteins is possible if model and intrinsic pK_a values and the matrix of ionizable site-site interactions of all ionizable sites are available (48–51). The model pK_a is an experimental quantity that corresponds to the ionization of a free ionizable site (amino acid) in solution. The intrinsic pK_a is a hypothetical quantity that corresponds to the pK_a of a specific ionizable site in the interior of the protein in the absence of interactions with other ionizable sites that are considered neutral. The apparent pK_a corresponds to interactions of an ionizable site with all other ionizable sites in their ionized form, given by a matrix of ionizable site-site interactions.

Intrinsic pK_a values were calculated using the method of Antosiewicz et al. (52, 53) implemented within the program UHBD (54, 55). The finite difference Poisson-Boltzmann solver of UHBD was used to calculate electrostatic potentials with continuum solvent representation. Apparent pK_a values were calculated using the clustering method (56) implemented within the program HYBRID (56). Dielectric constants of 78.4 and 20 were used for the solvent and protein interior (52) and temperature was set to 298K. The choice of the value of dielectric constant of 20 for the protein interior is optimal for the calculation of pK_a values within the computational protocol we used. It has been shown empirically that this dielectric constant yields better agreement with experimental pK_a values from a variety of protein and peptide systems and using crystal or solution structures (52, 53). The improved agreement with experimental data has been attributed to accounting for effects of conformational relaxation, specific ion binding, and tautomerization of neutral histidines and carboxylic acids that are not explicitly included in the computational models (an extensive discussion and comparison with other computational protocols can be found in Refs. 52 and 53). Ionic strengths spanning three orders of magnitude were used, corresponding to 15, 150, and 1500 mM concentrations. The parameter set of charges and van der Waals radii PARSE (57) was used. The finite difference focusing method (58, 59) was used in the calculations with five focusing grids of spacing-dimensions: 4 Å-64 × 64 × 64 Å^3, 2.5 Å-50 × 50 × 50 Å^3, 1.25 Å-30 × 30 × 30 Å^3, 0.5 Å-25 × 25 × 25 Å^3, 0.25 Å-20 × 20 × 20 Å^3. The solvent probe radius that defined the molecular surface was 1.4 Å. Dielectric smoothing at the protein-solvent interface (60) was used with an ion exclusion layer defined by a probe of 2.0 Å radius. The ionic strength dependence of the electrostatic potentials is calculated in the Boltzmann part of the Poisson-Boltzmann equation in the form of a variable that is a function of the Debye length (40). The ionic strength dependence of model pK_a values (61) is small in the salt concentration range we used and has not been taken into account in our pK_a calculation. Also, the dielectric constant of the solvent was kept the same. Our data show qualitatively the effect of ionic strength at 10-fold lower and 10-fold higher concentrations than the usual 150 mM of typical experiments. The dielectric constant of water drops only by 0–2% for 0–150 mM NaCl and by 19% for 1500 mM KCl (62).

Changes from the neutral to the charged state of ionizable residues were made by adding a +1 charge to the positively charged amino acids and a −1 charge to the negatively charged amino acids. Positive unit charges were added at the following atoms: the backbone amide of the N terminus, N_ζ of Lys, C_ζ of Arg, and N_δ of His when the initial hydrogen of neutral His is at N_ϵ, or N_ϵ of His when the initial hydrogen of neutral His is at N_δ. Negative unit charges were added at the following atoms: C_γ of Asp, C_δ of Glu, O_η of Tyr, and the backbone carbon of the C terminus. There are no reduced Cys residues in the structures used. The experimental model pK_a values used were: 12.0 for Arg, 10.4 for Lys, 9.6 for Tyr, 6.3 for His, 4.4 for Glu, 4.0 for Asp, 7.5 for the N terminus, and 3.8 for the C terminus.

Three structures were used in our calculations extracted from three different Protein Data Bank (PDB; Ref. 63) files with codes 1c3d for free C3d, 1ly2 for free CR2(SCR1–2), and 1ghq for the C3d-CR2(SCR1–2) complex. The crystallographic resolution of these structures is 1.8 Å, 1.8 Å, and 2.04 Å, respectively. Water and heteroatom groups were deleted from the PDB files and were not taken into account in our calculations. Heteroatom groups involve zinc ions (1ghq), glycans (1ly2, 1ghq), and glycerol (1c3d). To account for differences in the crystallographic structures because of 1) variable sequence length, 2) amino acid differences at the N terminus introduced by the protein expression method, and 3) differences because of lack of or incomplete crystallographic coordinates (owed to lack of electron density because of conformational flexibility), the following segments were used in the calculations: for free and bound C3d, residues Leu^2-Pro^{294} and Leu^2-Gln^{307}, respectively, were used. It should be noted that there is a sequence difference of 13 residues at the C-terminal region of free and bound CR2 in the crystallographic structures. The N and C termini of C3d are in spatial proximity and away from the association interface or the acidic pocket that are discussed in text. For free CR2, bound CR2(a), and bound CR2(b), residues Gln^1-Ile^{130}, Ala^1-Ser^{129}, and Ala^1-Glu^{134}, respectively, were used. It should be noted that the sequence of free CR2 was renumbered to Gln^1-Ile^{130} instead of Gln^0-Ile^{129}, after it was aligned against the sequence of bound CR2.

Addition of hydrogen atoms was made using the program WHAT IF version 99 (64). WHAT IF was also used to establish the initial protonation state of His, and flip states of His, Asn, and Gln residues, using the global hydrogen bonding network optimization option of the program (65, 66). Finally, WHAT IF was used to establish the neutral state of Asp, Glu, and

C terminus residues by adding a hydrogen atom at the $O_{\delta 2}$, $O_{\epsilon 2}$, and OXT atoms, respectively.

The fractional solvent accessible surface area (SASA) was calculated with the program MOLMOL (67) using a solvent probe radius of 1.4 Å, after removal of solvent and heteroatoms (water, glycerol molecules, Zn ions, and glycans) and after adding hydrogen atoms. We make these distinctions clear because different values of lost SASA upon association have been reported in Szakonyi et al. (19) and Prota et al. (22), but without specifying the parameters of the calculation.

Electrostatic potential calculations for isopotential contour plots were performed using the program GRASP (40, 68), with the PARSE parameter set (57), dielectric constants of 4 and 78.5 for the protein and solvent, respectively, solvent radius of 1.4 Å, in the absence of salt. In the structures used in these calculations, hydrogens were added and optimized for their hydrogen bonding network using WHAT IF (64, 66).

Molecular graphics have been created with the programs MOLMOL (67) and Swiss PDB Viewer (69).

Nomenclature compatibility between PDB, WHAT IF, UHBD, MOLMOL, and GRASP, and preparation for UHBD runs, was attained using a series of homemade PERL scripts.

Results and Discussion

We have performed pK_a calculations for free C3d (structure 1c3d), free CR2(SCR1–2) (structure 1ly2), and the C3d-CR2(SCR1–2) complex (structure 1ghq) to examine the experimentally observed ionic strength dependence of C3d-CR2 association (20, 33–36). The calculations were made at ionic strengths corresponding to 15, 150, and 1500 mM. We have predicted apparent pK_a values for each ionizable site of C3d, CR2(SCR1–2), and the C3d-CR2(SCR1–2) complex. Predicted pK_a values, based on three-dimensional crystallographic structures, provide us with a quantity of choice that can be easily interpreted both theoretically and experimentally.

Given the experimental evidence for the importance of mutations distant to the association interface for the binding ability of iC3b to CR2(SCR1–15) (35), we have also initiated a theoretical study to elucidate the role of these critical mutations on C3d-CR2(SCR1–2) binding.

Calculation of pK_a values, and ionic strength dependence of the C3d-CR2 association

Fig. 1*A* shows plots of the difference in the calculated apparent pK_a values between free C3d and C3d in complex with CR2(SCR1–2) at ionic strengths corresponding to 15, 150, and 1500 mM. Several ionizable residues show significant variations in pK_a values between free and bound C3d. A subset of these ionizable residues shows significant variations in pK_a values between free and bound C3d as a function of ionic strength. Residues marked with arrows in Fig. 1*A* will be discussed (vide infra). Table I summarizes the ionizable residues that show the largest differences at extreme ionic strength values corresponding to I = 15 and I = 1500 mM, using $\Delta pK_a = pK_a(\text{free})\text{-}pK_a(\text{complex})$ (1) and $\Delta\Delta pK_a = (\Delta pK_a)_{I=15} - (\Delta pK_a)_{I=1500}$ (2).

Differences $|\Delta\Delta pK_a| \geq 1$ are observed for 17 residues and differences in the range $0.5 \leq |\Delta\Delta pK_a| < 1$ are observed for 15 residues of a total of 77 ionizable residues (corresponding to C3d sequence length 1–294).

Fig. 1, *B* and *C*, show plots of the difference in the calculated apparent pK_a values between free CR2(SCR1–2) and in complex with C3d at ionic strengths corresponding to 15, 150, and 1500 mM. CR2(SCR1–2) is in dimer form in structure 1ghq, where only the first CR2(SCR1–2) is in contact with C3d (19). Fig. 1*B* shows the comparison between free CR2(SCR1–2) and the first CR2(SCR1–2) of structure 1ghq, called CR2(a). Fig. 1*C* shows the comparison between free CR2(SCR1–2) and the second CR2(SCR1–2) of structure 1ghq, called CR2(b). As expected, Fig. 1*B* shows more pronounced ΔpK_a and $\Delta\Delta pK_a$ differences because

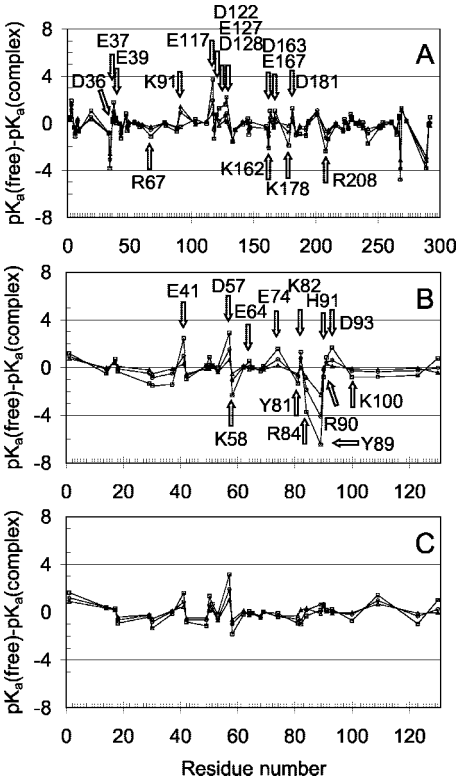

FIGURE 1. Ionic strength dependence of C3d-CR2(SCR1–2) association. Plots of $pK_a(\text{free})\text{-}pK_a(\text{complex})$ against residue number at ionic strengths corresponding to 15 mM (squares), 150 mM (circles), and 1500 mM (triangles) for (*A*) C3d (structures 1c3d, 1ghq), (*B*) CR2(SCR1–2) (structures 1ly2, 1ghq using CR2(a)), and (*C*) CR2(SCR1–2) (structures 1ly2, 1ghq using CR2(b)). Labels denote residues discussed in text that show perturbation of their pK_a values > 0.5 upon complex formation.

of the participation of CR2(a) in association with C3d. Differences $|\Delta\Delta pK_a| \geq 1$ are observed for 13 residues and differences in the range $0.5 \leq |\Delta\Delta pK_a| < 1$ are observed for 8 residues of a total of 32 ionizable residues. The differences in Fig. 1*C* are independent from the association of CR2(SCR1–2) with C3d. Table I summarizes the $\Delta\Delta pK_a$ differences. Residues marked with arrows in Fig. 1*B* will be discussed (vide infra).

The plots of Fig. 1 demonstrate the strong ionic strength dependence of C3d binding to CR2(SCR1–2) and depict the individual residues of C3d and CR2(SCR1–2) that are involved to, or affected by, binding. The origin of differences between pK_a(free) and pK_a(complex) is owed to intermolecular association that influences Coulombic interactions, desolvation, and structural changes. Additionally, structural differences of C3d and CR2(SCR1–2) in the crystallographic structures 1c3d, 1ly2, and 1ghq influence the pK_a values. These differences may be real or artifactual owed to crystal packing, variable chain length, mutations at the termini introduced by the expression method, crystallization conditions, data collection temperature, and interaction with heteroatoms from solvent molecules, metal ions, or glycosylation sites. Heteroatoms have not been included in the calculations but they may influence the conformation of specific residues in their vicinity.

Buried surface of the C3d-CR2 complex

We have calculated the buried surface area per residue of C3d and CR2(a) by substracting the fractional SASA of the C3d-CR2(SCR1–2) complex and individual components of the complex, C3d and CR2(a,b) all using coordinates from the structure 1ghq.

Table I. *Ionizable residues showing largest differences in ΔpK_a values at extreme ionic strengths*[a]

	Residues with $\Delta\Delta pK_a \geq 1$[b]	Residues with $0.5 \leq \Delta\Delta pK_a < 1$[b]
C3d[c]	N_{ter}, Tyr^{34}, $\underline{Glu^{37}}$, Lys^{91}, $\underline{\underline{\mathbf{Glu^{117}}}}$, Lys^{118}, $\mathbf{Asp^{122}}$, Glu^{127}, Asp^{128}, $\underline{Lys^{162}}$, $\underline{Glu^{167}}$, $\mathbf{Lys^{178}}$, $\mathbf{Asp^{181}}$, Arg^{208}, Tyr^{242}, Tyr^{268}, Tyr^{289}	Asp^{3}, Arg^{6}, Glu^{19}, Lys^{43}, Lys^{48}, Arg^{67}, Asp^{103}, Lys^{146}, Asp^{147}, $\underline{Asp^{163}}$, Tyr^{187}, Arg^{192}, Lys^{210}, Glu^{238}, $\underline{Asp^{292}}$
CR2(a)[d]	Arg^{29}, Tyr^{30}, Arg^{37}, Glu^{41}, Asp^{50}, Asp^{57}, Lys^{58}, $\mathbf{Glu^{74}}$, $\mathbf{Lys^{82}}$, $\mathbf{Arg^{84}}$, $\mathbf{Tyr^{89}}$, $\mathbf{Asp^{93}}$, C_{ter}	Arg^{14}, Glu^{64}, $\mathbf{Tyr^{81}}$, Arg^{90}, His^{91}, Lys^{100}, Lys^{109}, Arg^{123}
CR2(b)[e]	Glu^{41}, Asp^{50}, Asp^{57}, Lys^{58}, Lys^{82}, C_{ter}	N_{ter}, Tyr^{18}, Tyr^{30}, Lys^{49}, Lys^{51}, Asp^{53}, Tyr^{81}, Arg^{84}, Lys^{100}, Lys^{109}, Arg^{123}

[a] The quantity $\Delta\Delta pK_a$ is defined as: $\Delta\Delta pK_a = [pK_a(\text{free})\text{-}pK_a(\text{complex})]_{I=15} - [pK_a(\text{free})\text{-}pK_a(\text{complex})]_{I=1500}$, where I = 15 and I = 1500 correspond to extreme ionic strengths of 15 and 1500 mM.

[b] Underlined residues have been shown to affect iC3b-CR2(SCR1–15) association by Clemenza and Isenman (35). Doubly underlined residue corresponds to mutation by Szakonyi et al. (19). Residues in bold are located at the association interface.

[c] Calculation using structures of free C3d (1c3d) and C3d-CR2(SCR1–2) complex (1ghq). N_{ter}, N terminus.

[d] Calculation using structures of free CR2(SCR1–2) (1ly2) and C3d-CR2(SCR1–2) complex (1ghq). This comparison is with CR2(a), the first CR2(SCR1–2) of 1ghq that is in contact with C3d. C_{ter}, C terminus.

[e] Calculation using structures of free CR2(SCR1–2) (1ly2) and C3d-CR2(SCR1–2) complex (1ghq). This comparison is with CR2(b), the second CR2(SCR1-2) of 1ghq that is not in contact with C3d. N_{ter}, N terminus, C_{ter}, C terminus.

Fig. 2*A* shows a plot of the difference in SASA (ΔSASA) for C3d. This plot depicts three regions of C3d contiguous in space but not continuous in sequence, which are buried under the association interface of C3d with CR2(SCR1–2). These are segments 69–70, 112–122, and 170–186. The residues within these regions are: Leu^{116} ($30\% < \Delta SASA \geq 40\%$); Asn^{170}, Lys^{178}, Asp^{181} ($20\% < \Delta SASA \leq 30\%$); Pro^{69}, Ser^{70}, Glu^{117}, Pro^{121}, Asp^{122}, Ser^{171} ($10\% < \Delta SASA \leq 20\%$); Lys^{112}, Trp^{113}, Ile^{115}, Gln^{119}, Lys^{120}, Gly^{174}, Thr^{177}, Phe^{182}, Ala^{185}, Asn^{186} ($0\% < \Delta SASA \leq 10\%$).

Fig. 2*B* shows a plot of ΔSASA for CR2(a). This plot depicts the residues of CR2(a) that are buried under the association interface with C3d. These are: Ser^{86} ($30\% < \Delta SASA \leq 40\%$); Arg^{84} ($20\% < \Delta SASA \leq 30\%$); Tyr^{81}, Lys^{82}, Ile^{83}, Gly^{85}, Thr^{87}, Pro^{88} ($10\% < \Delta SASA \leq 20\%$); Glu^{74}, Asp^{93}, Lys^{100} ($0\% < \Delta SASA \leq 10\%$).

Our SASA calculations (described in *Materials and Methods*) showed an overall buried surface is 1422 $Å^2$, calculated using the structures of the complex C3d-CR2(SCR1–2).

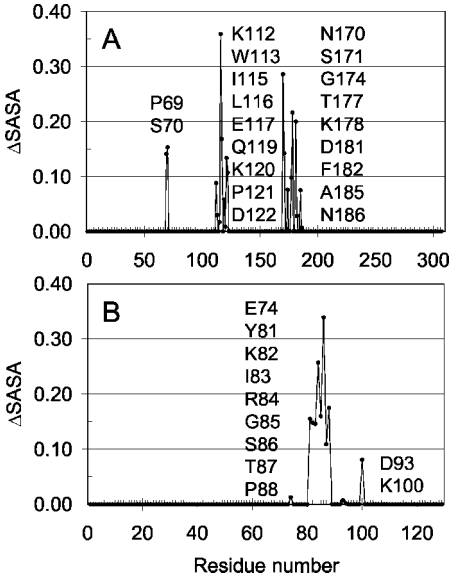

FIGURE 2. Buried surface area at the C3d-CR2(SCR1–2) association interface. Plots of the difference in SASA (ΔSASA) against residue number for (*A*) C3d from the structure 1ghq alone and in complex with CR2, and (*B*) CR2 from the structure 1ghq alone and in complex with CR2. CR2(a) of 1ghq has been used that is in contact with C3d. Labels denote residues with nonzero ΔSASA. Labels are arranged from top to bottom for each envelope of peaks corresponding to increasing residue number.

Origin of apparent and model pK_a differences

Table II shows lists of calculated (apparent) pK_a values at ionic strength of 150 mM for the ionizable sites summarized in Table I (a complete set of appraent pK_a values is given in Tables I to III of supplemental material).[4] Model pK_a values of free amino acids in solution are also given in Table II for comparison. In most data, there is a larger apparent than model pK_a value for basic residues and a smaller apparent than model pK_a value for acidic residues. These trends are indicative of favorable Coulombic interactions between basic and acidic residues with their charge sites in proximity, typically in the form of salt bridges or hydrogen bonds. However, in certain instances opposite trends are observed, where smaller apparent than model pK_a values for basic residues and larger apparent than model pK_a values for acidic residues are observed. These are cases of unfavorable Coulombic interactions, such as when two basic residues are in proximity with each other or two acidic residues are in proximity with each other. Similar shifts in apparent pK_a values can also be present in situations of unfavorable interactions with the environment, as is the case of desolvation of ionizable residues that are found in the interior of the protein. Because most ionizable residues in the protein are deprived from solvent to a certain degree, the unfavorable desolvation effect is always present and it is either compensated or surpassed by the effect of favorable Coulombic interactions, or it is further strengthened by the effect of unfavorable Coulombic interactions. The latter is much less frequent than the former.

Origin of ionic strength effect

The overall trend of the results of Fig. 1 demonstrates that the differences in the apparent pK_a values between free and bound species increase as the ionic strength decreases. This points to the significance of the underlying electrostatic interactions for association and is particularly obvious for the residues marked in Fig. 1 that are located at, and away from, the association interface that contribute to binding (vide infra). At low ionic strength, association is stronger because shielding of electrostatic interactions by solvent salt molecules is not as effective as at high ionic strength. This is in agreement with recent experimental data using surface plasmon resonance that showed increase in ionic strength weakened C3dg-CR2(SCR1–2) interaction (20) and C3d-CR2(SCR1–15) interaction (36). In addition, Guthridge et al. (20) have shown that C3dg-CR2(SCR1–2) association is weakened at low pH. This

[4] The on-line version of this article contains supplemental material.

Table II. *Calculated apparent pK_a values for ionizable residues that show significant ionic strength dependence (summarized in Table I)*[a]

	Residue No.	Residue	Model pK_a	Apparent pK_a Free	Apparent pK_a Complex
C3d	2	Leu-N_{ter}[b]	7.5	7.3	6.9
	3	Asp	4	3.2	1.6
	6	Arg	12	14.3	15.1
	19	Glu	4.4	1.1	0.5
	34	Tyr	9.6	13.3	16.4
	37	Glu	4.4	3.7	2.8
	43	Lys	10.4	11.1	12.0
	48	Lys	10.4	10.3	10.6
	67	Arg	12	13.3	13.9
	91	Lys	10.4	17.3	16.4
	103	Asp	4	2.7	2.7
	117	Glu	4.4	4.4	2.4
	118	Lys	10.4	12.1	12.6
	122	Asp	4	3.4	3.2
	127	Glu	4.4	0.6	−0.1
	128	Asp	4	2.7	1.8
	146	Lys	10.4	10.8	11.3
	147	Asp	4	2.5	2.8
	162	Lys	10.4	11.7	12.9
	163	Asp	4	3.7	3.2
	167	Glu	4.4	4.3	3.9
	178	Lys	10.4	11.3	12.1
	181	Asp	4	3.6	3.1
	187	Tyr	9.6	14.5	14.9
	192	Arg	12	14.6	15.1
	208	Arg	12	15.0	16.2
	210	Lys	10.4	10.4	11.1
	238	Glu	4.4	0.9	1.2
	242	Tyr	9.6	20.1	21.0
	268	Tyr	9.6	12.2	16.1
	289	Tyr	9.6	10.9	14.1
	292	Asp	4	4.2	4.1
CR2					
	14	Arg	12	12.3	12.4
	29	Arg	12	12.3	12.7
	30	Tyr	9.6	13.6	14.5
	37	Arg	12	13.2	13.7
	41	Glu	4.4	2.6	1.6
	50	Asp	4	2.9	2.6
	57	Asp	4	2.7	1.2
	58	Lys	10.4	11.6	12.7
	64	Glu	4.4	2.4	2.4
	74	Glu	4.4	3.1	2.5
	81	Tyr	9.6	9.8	10.6
	82	Lys	10.4	11.8	11.0
	84	Arg	12	12.8	14.7
	89	Tyr	9.6	11.4	15.5
	90	Arg	12	13.3	13.5
	91	His	6.3	5.0	4.5
	93	Asp	4	3.2	2.6
	100	Lys	10.4	10.4	10.7
	109	Lys	10.4	10.2	10.6
	123	Arg	12	12.1	12.4
	129/130	Ser-C_{ter}/Ile-C_{ter}[c]	3.8	4.0	4.0

[a] Ionic strength of the calculations presented here corresponds to 150 mM. A complete set of apparent pK_a values is given in Tables I to III of supplemental material.

[b] Denotes the N-terminal positive charge. N_{ter}, N terminus.

[c] Denotes the C-terminal negative charge C_{ter}, C terminus.. It should be noted that the end residue of CR2(a) in the structure of the complex (1 ghq) is Ser^{129} and the end residue of CR2 in the free structure (1ly2) is Ile^{130}.

can be attributed to protonation (neutralization) of acidic side chains that at high pH participate in charge-charge interactions, involving two or more charges. This is particularly important in case of the overall electrostatic potential of C3d, which is predominantly of negative character (vide infra).

The C3d-CR2 association interface

Fig. 3*A* shows a ribbon representation of the C3d-CR2(SCR1–2) complex (19) with superimposed free C3d (39) and free CR2(SCR1–2) (22). In the structure of the complex, CR2(SCR1–2) is in dimer form with only the first CR2(SCR1–2) molecule, CR2(a), being in contact with C3d. The variable length at the C terminus between free and bound C3d is also depicted in Fig. 3*A*. C3d is an all-helical protein forming an α-α barrel structural motif (39). The structure of CR2(SCR1–2) comprises the first 2 of 15 or 16 SCR domains and is an all-beta sheet protein. Each SCR domain forms a β-barrel structural motif (70).

The C3d-CR2(SCR1–2) crystal structure has revealed shape complementarity between C3d and CR2(SCR1–2), an extensive network of hydrogen bonds (some mediated by water molecules), and the presence of an anion hole in C3d (19). The anion hole is formed by residues Ile^{115}, Leu^{116}, Glu^{117}, and Gln^{119} of C3d and is occupied by positively charged residue Arg^{84} of CR2(SCR1–2) (19). Fig. 3*B* depicts ionizable residues of the C3d-CR2(SCR1–2) complex that are potential participants in electrostatic interactions, including an ionizable residue channel in C3d that starts from the anion hole of the association interface and terminates at a diametrically opposite end in close spatial proximity to the termini.

Our findings demonstrate significant differences in the pK_a values between free and bound C3d and CR2(SCR1–2) not only localized at the sites of association, but also spanning the length of the molecules (Figs. 1 and 3, *A–E*). The association interface at the C3d side contains buried ionizable residues Lys^{112}, Glu^{117}, Lys^{120}, Asp^{122}, Lys^{178}, and Asp^{181}, (Fig. 2*A*); and at the CR2 side contains ionizable residue Tyr^{81}, Lys^{82}, Arg^{84}, Asp^{93}, and Lys^{100} (Fig. 2*B*). Our data show strong ionic strength dependence for residues at the association interface Glu^{117}, Asp^{122}, Lys^{178}, Asp^{181} of C3d, and Glu^{74}, Tyr^{81}, Lys^{82}, Arg^{84}, Asp^{93}, Lys^{100} of CR2 (Figs. 1, *A* and *B*, and 2; Table I). From these residues, Glu^{117}, Lys^{178} of C3d, and Glu^{74}, Arg^{84}, Asp^{93} of CR2 also show sizeable perturbations in their pK_a values upon complex formation (Fig. 1, *A* and *B*; Table II). This is in agreement with the observation of Szakonyi et al. (19) that "residues Lys^{178} of C3d and Arg^{84}, Lys^{100} of CR2 should be sensitive to salt concentration," but our data demonstrate that additional residues in the vicinity or away from the association interface should also be sensitive to salt concentration (Fig. 1, *A* and *B*; Table II). Networks of electrostatic interactions and desolvation are responsible for the calculated ionic strength dependence and pK_a perturbations, rather than isolated pairs of ionizable sites. Of particular interest is the pair Glu^{117}(C3d)-Arg^{84}(CR2) that shows some of the largest differences between free and bound structures and of the largest ionic strength dependencies (Fig. 1, *A* and *B*; Table II). In solution, this can be attributed to a strong Coulombic interaction in the form of a salt bridge between the two residues that stabilize the complex interface. However, in the C3d-CR2(SCR1–2) complex structure one nonphysiological zinc ion is in close proximity to Glu^{117} that possibly affects the distance between the ionizable sites of Glu^{117}(C3d)-Arg^{84}(CR2) in the crystallographic structure (19, 22). The zinc atoms of structure 1ghq are not included in our calculations.

Interestingly, elimination of Glu^{117} in a Leu^{116}Ala/Glu^{117}Ala mutant inhibited the binding ability of plate-bound C3d with full-length CR2 to the same extent as wild-type protein, using ELISA competition experiments; however, introduction of positive charges in mutants Ile^{115}Arg/Leu^{116}Arg/Asn^{170}Ala and Asn^{170}Arg resulted in little or no inhibition (19). These results do not directly implicate the

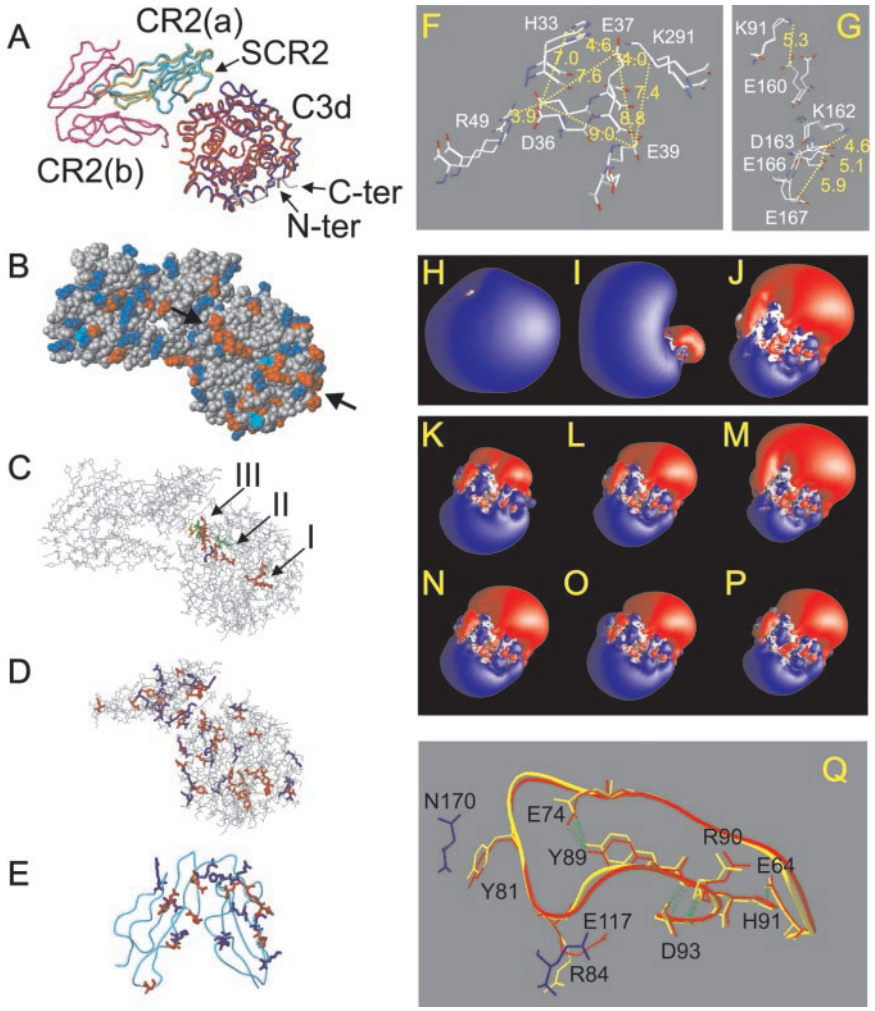

FIGURE 3. *A–E*, Relative topology of C3d and CR2 and location of C3d and CR2 residues discussed in text. *A*, Tube representation of the superposition of structure of the C3d-CR2(SCR1–2) complex with free C3d (1ghq and 1c3d, respectively), and the C3d-CR2(SCR1–2) complex with free CR2(SCR1–2) (1ghq and 1ly2, respectively) using the backbone heavy atoms. Free C3d is drawn in blue; bound C3d is drawn in red with the exception of the additional 13 C-terminal residues (not present in the structure of free C3d) that are drawn in gray; free CR2 is drawn in orange; bound CR2(a) is drawn in cyan; and bound CR2(b) is drawn in magenta. The N (N-ter) and C (C-ter) termini are marked with arrows to show their spatial proximity. *B*, A van der Waals surface representation of the C3d-CR2(SCR1–2) complex (structure 1ghq) with acidic residues Asp, Glu, and C-ter drawn in red, basic residues Arg, Lys, and N-ter drawn in blue, and His drawn in light blue. The ionizable residue channel is shown between the arrows. *C*, The C3d-CR2(SCR1–2) complex with experimentally mutated residues discussed in text (Clemenza and Isenman, Ref. 35; Szakonyi et al., Ref. 19), depicted in different colors and thicker bond lines. Arrows show mutated residues within the two clusters of the acidic channel (I: the Asp^{36}/Glu^{37}/Glu^{39} cluster; II: the Glu^{160}/Lys^{162}/Asp^{163}/Ile^{164}/Glu^{166}/Glu^{167}) and the cluster at the association interface (III: Ile^{115}/Leu^{116}/Glu^{117}/Asn^{170}). *D*, The C3d-CR2(SCR1–2) complex with ionizable residues that show perturbation of their pK_a values upon complex formation (pK_a(free)-pK_a(complex) > 0.5), depicted in different colors and thicker bond lines. *E*, The structure of free CR2(SCR1–2) with ionizable residues that participate in SCR1/SCR2 packing and in CR2-C3d association depicted in different colors and thicker bond lines. In *B–E*, red denotes acidic residues, blue denotes basic residues, yellow denotes neutral polar residues, and green denotes hydrophobic residues. In *E*, only side chains discussed in text are shown and the rest are deleted for clarity. *F* and *G*, Structural differences between free and CR2(SCR1–2)-bound C3d within the two clusters of the ionizable residue channel discussed in text. *F*, Multiresidue electrostatic interactions, including salt bridges, for residues Asp^{36}, Glu^{37}, and Glu^{39} of cluster I. *G*, Multiresidue electrostatic interactions, including salt bridges, for residues Glu^{160}, Lys^{162}, Asp^{163}, Glu^{166}, and Glu^{167} of cluster II. The backbone heavy atoms of C3d residues 1–294 in structures 1c3d and 1ghq were used for the superposition. Key distances (in Å) are marked using residues of bound C3d. *H–P*, Isopotential contour representation at $\pm$ 1 k_BT (where k_B is the Boltzmann constant and T is the temperature) for C3d, CR2(SCR1–2), and C3d-CR2(SCR1–2) and effect of mutations within the ionizable residue channel on the electrostatic potential of C3d. *H*, Free CR2(SCR1–2) using structure 1ly2. *I*, The C3d-CR2(SCR1–2) complex using structure 1ghq. Both CR2 molecules, CR2(a,b), of the complex were used. *J*, Free C3d using structure 1c3d. *K*, Asp^{36}Ala/Glu^{37}Ala/Glu^{39}Ala C3d mutant. *L*, Asp^{163}Ala C3d mutant. *M*, Lys^{162}Ala C3d mutant. *N*, Leu^{116}Ala/Glu^{117}Ala C3d mutant. *O*, Ile^{115}Arg/Leu^{116}Arg/Asn^{170}Ala C3d mutant. *P*, Asn^{170}Arg C3d mutant. Theoretical mutations represented in (*K–M*) are distant to the association interface while those in (*N–P*) are located at the association interface. Blue and red denote positive and negative, respectively, potential. The orientation of CR2(SCR1–2) is the same in *H* and *I*. The orientation of C3d is the same in panels *J–P*. The electrostatic potential calculations were performed using the same conditions for all panels. The box size in *K–P* is also identical. *Q*, The electrostatic interdependence of ionizable residues of CR2(SCR1–2) that affects CR2(SCR1–2)-C3d binding. Residues Glu^{64}, His^{91}, Arg^{90}, Asp^{93}, Tyr^{89}, Glu^{74}, Asp^{93} of free CR2 (in red) and bound CR2 (in yellow) participate in the SCR1/SCR2 packing. CR2 residues Arg^{84} and Tyr^{81} interacting with C3d residues Glu^{117} and Asn^{170} (in blue), respectively, are also shown. Hydrogen bonds are shown in green dashed lines.

side chain of Glu^{117} in association, but demonstrate the significance of negative charge or neutrality on the C3d side of the association interface (Fig. 3*B*). They are suggestive that the overall electrostatic character of the C3d-CR2 association interface is responsible to maintain association in addition to, or instead of, individual ion pairs at the association interface. We will also present

below, that the overall electrostatic character throughout the volume of the individual molecules of C3d and CR2 is important for association.

The role of the ionizable residue channel of C3d in binding

C3d is a globular protein with a predominantly hydrophobic core; however, several polar residues point into the core stabilized by hydrogen bonds to buried water molecules (39). In addition, a patch of surface-exposed hydrophobic residues is observed in the site of formation of the thioester bond responsible for covalent attachment (39). These residues are highly conserved among different species. It should be noted that the residue of covalent attachment, Cys^{17}, has been mutated to Ala in the crystallographic structures (19, 39). Finally, an extended acidic pocket was observed on the surface of C3d, consisting of predominantly nonconserved residues. The acidic pocket, first observed by Nagar et al. (39), is indeed part of an ionizable residue channel as mentioned above (Fig. 3*B*).

The authors of the free C3d structure proposed that the acidic pocket may be the association site of C3d with CR2 (39). Subsequently, Clemenza and Isenman (35) demonstrated that single, double, or triple mutations of charged residues within the acidic pocket are responsible for modulating the binding of C3d-containing iC3b to full-length CR2. They identified two charged amino acid clusters within the acidic pocket, the first comprising residues Asp^{36}, Glu^{37}, and Glu^{39} and the second comprising residues Glu^{160}, Lys^{162}, Asp^{163}, Glu^{166}, and Glu^{167}. Specifically, in the first cluster the mutants Glu^{37}Ala, Glu^{39}Ala, Asp^{36}Ala/Glu^{37}Ala, Asp^{36}Ala/Glu^{39}Ala, Glu^{37}Ala/Glu^{39}Ala, Asp^{36}Ala/Glu^{37}Ala/Glu^{39}Ala, and Asp^{36}Asn/Glu^{37}Gln/Glu^{39}Gln resulted to >50% loss in binding ability (35). The triple mutants, Asp^{36}Ala/Glu^{37}Ala/Glu^{39}Ala and Asp^{36}Asn/Glu^{37}Gln/Glu^{39}Gln, were the most effective bringing the binding ability to <20% (35). In the second cluster, the mutants Glu^{160}Ala, Asp^{163}Ala, Asp^{163}Asn, Glu^{166}Ala, Glu^{160}Ala/Asp^{163}Ala, Asp^{163}Ala/Glu^{166}Ala, Glu^{166}Ala/Glu^{167}Ala resulted in >50% loss in binding ability (35). The mutants Asp^{163}Ala, Asp^{163}Asn, and Glu^{160}Ala/Asp^{163}Ala were the most effective, bringing the binding ability to <5%. All of the above mutations involved removing acidic residues. Interestingly, replacement of a hydrophobic residue also resulted in <5% binding ability in the Ile^{164}Ala mutant (35). A dramatic effect was observed when the positive charge of the pocket was removed, which resulted in a 2-fold increase in the binding ability of the mutant Lys^{162}Ala (35). These results indicated that an overall negative character of C3d was the basis for association with CR2 and led the authors of this study to suggest that the mutated acidic residues were the contacts between C3d and CR2 (35). However, the structure of the C3d-CR2(SCR1–2) complex revealed that the mutated acidic pocket residues were remote to the association interface (19). Fig. 3*C* shows the relative topology of key residues from the Clemenza and Isenman (35) acidic pocket mutants to the association interface.

Our study demonstrates significant ionic strength dependencies for some of the residues of the ionizable residue channel, which were mutated by Clemenza and Isenman (35). Specifically, ionic strength dependence is observed for Glu^{37} but not for Asp^{36} and Glu^{39} within the first cluster, and for Lys^{162}, Asp^{163}, Glu^{167} but not Glu^{160} and Glu^{166} within the second cluster (Fig. 1*A*, Table I). In addition, Glu^{37}, Lys^{162}, and Asp^{163} show ΔpK_a's >0.5 between free and complex C3d (Table II). Fig. 3*D* shows the relative topology to the association interface of the ionizable residues of C3d with significant ionic strength dependence in their pK_a values (Table I). Based on the pK_a differences, it appears that the ionizable residues of the channel are either affected by or contribute to association. It is also possible that differences in pK_a values calculated using the structures of free and bound C3d are not only because of association but also because of small structural differences induced by crystal packing forces. Fig. 3, *F* and *G*, shows such differences for the two clusters of the ionizable residue channel, but also Fig. 3, *F* and *G*, shows the strong Coulombic interdependence (both favorable and unfavorable) among the ionizable side chains of the channel. Given the experimental evidence that residues depicted in Fig. 3, *F* and *G*, are responsible for loss or enhancement of binding ability, despite their remoteness to the association site (35), we have investigated their contribution to the overall electrostatic potential of C3d.

Fig. 3, *H–P*, shows plots of the calculated isopotential contour surfaces for free C3d, free CR2(SCR1–2), and the C3d-CR2(SCR1–2) complex. Isopotential contour plots provide a visual interpretation of the spatial distribution of electrostatic potentials at equal value, which can be intuitively translated into electric fields. It is apparent that CR2(SCR1–2) is predominantly positively charged (Fig. 3*H*) and C3d is predominantly negatively charged (Fig. 3*J*), which suggests that the recognition and acceleration of binding is electrostatic in nature. This charge composition is reflected in the C3d-CR2(SCR1–2) complex, which has mixed character resembling a macrodipole spanning the volume of the complex with a predominantly positive end toward CR2 and a negative end toward C3d (Fig. 3*I*).

To assess the contribution of the mutations of Clemenza and Isenman (35) on the electrostatic potential of C3d, we constructed the theoretical mutations Asp^{36}Ala/Glu^{37}Ala/Glu^{39}Ala, Asp^{163}Ala, and Lys^{162}Ala, using the three-dimensional structures of free C3d and the C3d-CR2(SCR1–2) complex. We have used these structures to calculate the effect of each mutation on the overall electrostatic potential. Fig. 3, *K–M*, shows plots of the isopotential contours superimposed on the structures of the Asp^{36}Ala/Glu^{37}Ala/Glu^{39}Ala, Asp^{163}Ala, and Lys^{162}Ala mutants. Fig. 3, *K* and *L*, shows significant loss of the negative character of the electrostatic potential of the theoretical mutants Asp^{36}Ala/Glu^{37}Ala/Glu^{39}Ala and Asp^{163}Ala when compared with wild type (Fig. 3*J*), which we propose to be responsible for the experimentally observed loss in binding ability. To the contrary, the significant increase of the negative character of the electrostatic potential upon removal of positively charged Lys^{162} (Fig. 3*M*) compared with wild type (Fig. 3*J*) is responsible for the increased binding ability of mutant Lys^{162}Ala.

We also constructed another set of theoretical mutants from a different experimental study (19), namely Asn^{170}Arg, Ile^{115}Arg/Leu^{116}Arg/Asn^{170}Ala, and Leu^{116}Ala/Glu^{117}Ala. In competition experiments, wild-type C3d and mutant Leu^{116}Ala/Glu^{117}Ala C3d were able to bind to full-length CR2 similarly, while mutants Asn^{170}Arg, Ile^{115}Arg/Leu^{116}Arg/Asn^{170}Ala had lost most of their binding capabilities (19). Both the Asn^{170}Arg and Ile^{115}Arg/Leu^{116}Arg/Asn^{170}Ala mutants have introduced positive charge(s) in the association interface of C3d and CR2. The Leu^{116}Ala/Glu^{117}Ala mutant removed the negative charge of Glu^{117} and eliminated a hydrogen bond involving its side chain. All Ile^{115}, Leu^{116}, Glu^{117}, and Asn^{170} are buried at the C3d-CR2 association interface (Fig. 2*A*). Fig. 3*C* shows the relative topology of these residues to the association interface. In addition, Glu^{117} is one of the residues that shows the strongest ionic strength effect in the pK_a calculations (Fig. 1*A*). Fig. 3, *N–P*, shows the isopotential contours for the three mutants. All three mutants have reduced negative character compared with wild type shown in Fig. 3*J*. This effect is more pronounced in the Ile^{115}Arg/Leu^{116}Arg/Asn^{170}Ala or Asn^{170}Arg and mutants that showed little or no inhibition of binding for full-length CR2 with plate-bound wild-type C3d, and

less pronounced in the $Leu^{116}Ala/Glu^{117}Ala$ mutant that showed comparable inhibition of binding as the wild type (19). The effect of the $Leu^{116}Ala/Glu^{117}Ala$ mutation on the isopotential contours of C3d is small but evident (Fig. 3*N*) and we would expect that it should affect binding to C3d to some extent. It is possible that the dynamic range of the immunologic assay of the competition experiment (19) is not sufficient to measure subtle changes in binding.

The data presented in Fig. 3, *H–P*, suggest that the association between C3d and CR2(SCR1–2) is initiated and accelerated by Coulombic interaction between the predominantly negative C3d and the predominantly positive CR2. Mutations on the C3d side that result in altering the negative electrostatic potential, and the electric field associated with it, are responsible for reduced, diminished, or enhanced binding to CR2(SCR1–2). However, the final step of association between C3d and CR2(SCR1–2) does not involve the energetically unfavorable desolvation of charged residues. The crystallographic structure of the C3d-CR2(SCR1–2) complex shows that the association interface of the two molecules is stabilized by hydrophobic, van der Waals, and main chain hydrogen-bonding interactions, which is an energetically more favorable arrangement. From these observations we can assume that the association rate is dominated by the electrostatic potentials of C3d and CR2, while the dissociation rate is controlled by the presence of hydrogen bonds, van der Waals interactions, and hydrophobicity at the association interface. Additional theoretical studies to quantitate association rates are currently in progress.

We are aware of another study that has reported on the significant effects of charges on association, when the charges are not located on the association interface. Specifically, Selzer et al. (71) were successful in increasing the association of TEM1 β-lactamase with its protein inhibitor BLIP, by strategically positioning charged residues on BLIP in such a way that the resulting electrostatic fields enhanced the k_{on} rate while leaving the k_{off} rate unchanged. The researchers of that study designed several mutants with enhanced affinity with, most spectacular, a 250-fold increase.

Length of C3d

Some of the remaining ΔpK_as and ionic strength differences at the N and C termini, which are in proximity (Fig. 3, *A* and *D*), may be owed to the different length in the free and bound C3d structures. Indeed, pK_a calculations using only the first 294 residues of C3d from the structure of the complex demonstrate that pK_a values in the segments 1–34 and 242–294 are affected by the presence (or lack) of the 13 C-terminal residues (data not shown). The effects of these regions in the pK_a values or in the plotted electrostatic potentials are not discussed in text, because they may be artifactual.

SCR1/SCR2 packing in CR2

Fig. 3*E* shows a backbone ribbon representation of the structure of free CR2(SCR1–2) (22) with overlaid side chains that show significant ionic strength dependence of the pK_a differences between free and bound species (Table I). The two SCR domains form a V-shaped structure with substantial degree of flexibility mediated by the long interdomain linker (22). This flexibility is responsible for the interdomain angle and also for the relative orientation of the principal components of the ellipsoids representing the SCR domains (23–29, 31, 32) and in the case of CR2 it promotes the interaction with C3d (19, 22).

The SCR domains in general have a conserved small hydrophobic core structure. Two SCR domains are linked through a short three to eight residue linker that allows mobility of the SCR domains, with the first two SCRs of CR2 having the longest linker known. The combination of two domains can be linear or variable angle V-shaped, but also the relative orientation of the principal components of the ellipsoids representing the SCR domains can be variable. The two first SCRs of CR2, in both free and C3d-bound forms, are V-shaped with packing dominated by hydrophobic interactions, as opposed to most SCR domains in known structures that are closer to linear (19, 22, 23–29, 31, 32). Apparently the eight-residue long linker of the first SCR pair of CR2 allows for the hydrophobic packing of the two domains of CR2, which in turn allows for binding to C3d through the second SCR domain (19). This was a rather surprising result as it has been shown that both SCR domains are necessary for C3d binding (13, 14, 16, 18, 20).

The SCR1/SCR2 packing in CR2 is mainly through hydrophobic contacts involving Ile^{38}, Trp^{11}, and Pro^{120}, but also through a salt bridge between Glu^{64} and His^{91} (22). Prota et al. (22) have suggested that this type of SCR1/SCR2 packing has an allosteric effect on CR2-C3d association through a network of intramolecular, interdomain contacts. The end result is the proper orientation of Arg^{84} and Tyr^{81} to form intermolecular contacts with Glu^{117} and Asn^{170} of C3d (Fig. 3*Q*). Fig. 1*B* demonstrates that Glu^{64}, His^{91}, Arg^{84}, and Tyr^{81} show significant ionic strength dependence. It should be noted that Arg^{84}, hydrogen bonded Glu^{74}-Tyr^{89}, and nearby Arg90 and Asp^{93}, show some of the largest ionic strength dependencies (Fig. 1*B*). The spatial arrangement of these residues suggests a complex electrostatic interdependence of ionizable residues Glu^{64}-His^{91}-Asp^{93}-Arg^{90}-Tyr^{89}-Glu^{74} involving main or side chain hydrogen bonds (Fig. 3*Q*). This may be responsible for the reported subtle movement for Arg^{90} and His^{91} of 0.5–0.8 Å away from the C3d binding site upon formation of the complex (22). It has been suggested by Prota et al. (22) that the movement of these two residues may be responsible for pulling the linker and the SCR1 domain with them, thus providing a link between SCR1 and the C3d binding site of SCR2. In this sense, the packing of SCR1/SCR2 is important in mediating C3d-CR2 binding (22).

It should be noted that possible effects from the glycan attached to Asn^{101} (of SCR2) and a second glycan, reported in the crystallographic structure of free CR2 only, attached to Asn^{107} have not been directly modeled into our pK_a calculations. The absence of a second glycosylation site in complexed CR2 would make this comparison difficult. However, the effect of glycans in altering the local structure is implicitly built into our pK_a calculations by the specific conformations of their attached residues.

Length of CR2

It should be noted that the binding experiments of CR2 with mutated C3d were performed using the full-length soluble CR2 with C3d (19) and full-length CR2 on Raji cells with iC3b (35). Our theoretical mutations and calculations were performed using C3d and the first two SCRs only (SCR1/SCR2), which are present in the crystallographic structures. It has been experimentally shown that the first two SCRs are essential for binding to C3d, despite the fact that only SCR2 contacts C3d. We have discussed above the hypothesis on the contribution of the SCR1 domain in binding (22). However, it should not be excluded that additional interactions with C3d from subsequent SCRs in CR2 may be affecting association. This possibility has been suggested by kinetic studies using surface plasmon resonance (20, 36). The kinetic studies have shown a similar binding affinity for CR2(SCR1–2) and CR2(SCR1–15) with C3d, but slower association and dissociation rates for CR2(SCR1–15) compared with CR2(SCR1–2) (20). This could be attributed to altered overall electrostatic character in the full-length CR2 (e.g., less positive charge or spatially delocalized charge) compared with CR2 with only the first two SCR domains, or to additional site(s) of interaction. An additional potential site of

C3d for interaction with full-length CR2 could include the sequence segment Glu^{228}-Asp-Pro-Gly-Lys-Gln-Leu-Tyr-Asn-Val-Glu-Ala^{239}, which is not located within the ionizable residue channel. This site was first proposed by peptide mapping studies (72) and was confirmed by surface plasmon resonance studies (36). The presence of this binding site was also supported by site-directed mutagenesis studies within this site, in which simultaneous multiple replacements resulted to ~20% reduction in binding ability relative to wild type (34). This could be possible if the 15 or 16 SCRs of CR2 form a flexible chain that folds over and contacts C3d. In this case, additional contacts with the ionizable residue channel could be present and may contribute to the binding effects of the ionizable residue channel mutations (35). In the absence of crystallographic data with full-length CR2, we cannot address the possibility theoretically. Additional contacts of full-length CR2 with iC3b outside the C3d segment may also be present. We should point out though that the ionic strength dependence of C3d-CR2 association has been measured experimentally in CR2(SCR1–2) and CR2(SCR1–15) (20, 36).

Assessment of methodology

The crystallographic atomic coordinates are defined within a resolution range. Higher resolution does not necessarily mean more accurate atomic representation, because the crystallographic structures are quasistatic structures that do not reflect the true dynamic character of the proteins or protein complexes. This is a potential source of errors for the calculation of electrostatic potentials and pK_a values. Theoretically, more accurate representation of proteins and protein complexes is possible by performing molecular dynamics simulations at long time scales and electrostatic calculations for individual snapshots of the dynamics trajectories. However, even without molecular dynamics, an increasing number of electrostatic calculation studies, based on crystallographic structures, have aided to understand experimental data. The capabilities of electrostatic calculations have been reviewed in Refs. 40 and 73–79. The effect of small variations of the atomic positions on the calculated pK_a values has been demonstrated using structural ensembles derived from nuclear magnetic resonance (NMR) data (53, 80). The NMR ensemble is characterized by the root mean square deviation of the atomic coordinates, which defines the precision (but not accuracy) of the structure. Calculated pK_a values using NMR structural ensembles can also be defined within a root mean square deviation (53, 80). It has been shown that pK_a values calculated using NMR structures are only in slightly better agreement with experimental data than pK_a values calculated with crystallographic structures, possibly owed to the more realistic conformational space spanned by the NMR structures (53).

In our study, we have constructed theoretical mutants of C3d using the crystallographic structure of C3d, under the assumption that the overall fold of C3d remained the same in the theoretical mutants as in native C3d. Our goal was simply to evaluate the contribution of the mutated residues to electrostatic interactions and the resulting electrostatic potentials and pK_a values, in the given conformation of native C3d. For this reason, we have not used the theoretically mutated structures in a quantitative way to calculate their pK_a values or association constants. In reality, local or global conformational changes may or may not occur upon mutation, depending on how radical or how conservative the mutation is and on the participation of the mutated residue to structure formation and stability. If our goal was to use the mutated structures in a more quantitative way, they should have been subjected to molecular dynamics simulations. However, this was not the goal of our study.

The ultimate judge for the effectiveness of the electrostatic calculations is comparison with experimental data. We believe that prediction of measurable physical parameters using electrostatic calculations is a unique way to explain the physical basis of biological structure and function, when electrostatics play a significant role. We also believe that predictions based on calculations can be useful and efficient guides, in terms of time and effort, for experimental studies. Finally, we should note that efforts to further improve the physical and computational performance of the algorithms, used in the electrostatic calculations, are continuous among biophysicists and biophysical chemists.

Summary

We studied the nature of the interaction between complement component C3d and complement receptor CR2. It has been recognized, based on experimental data, that the association is strongly dependent on ionic strength and on pH. The solution of the three-dimensional structure of the complex of C3d-CR2(SCR1–2) has revealed the sites of association of the two molecules, which are dominated by the presence of hydrogen bonds. This is in agreement with mutagenesis studies on the C3d site of interaction and can explain to a certain extent the significant ionic strength dependence of C3d-CR2 binding. However, additional mutagenesis studies aiming to disrupt a negatively charged cavity of C3d away from the site of interaction with CR2 have resulted in altered C3d-CR2 binding. To understand the role of charges in C3d-CR2 association, we performed electrostatic calculations based on the solution of the finite difference linearized Poisson-Boltzmann equation with an averaged continuous solvent representation. We used the molecular detail of crystallographic structures of free C3d, free CR2(SCR1–2), and the C3d-CR2(SCR1–2) complex to perform our calculations at a protein atomic level. The electrostatic interactions among all ionizable residues of C3d and C3d-CR2 were determined in the form of electrostatic potentials, ionization free energies, and ultimately apparent pK_a values, which provide us with a quantity that can be easily interpreted both theoretically and experimentally. Our studies suggest that the association of C3d with CR2 is predominantly electrostatic in nature and involves the whole molecules and not only the limited association sites. This means that recognition and binding is owed to electrostatic attraction (controlling k_{on}) and that van der Waals and hydrogen bonding interactions are responsible for making the two molecules stick together (mainly controlling k_{off}). In particular, charged residues at regions of C3d remote to the association site appear to affect the binding with CR2. Our results are in qualitative agreement with the earlier surface plasmon resonance studies that addressed the pH and ionic strength dependence of C3d-CR2 association. They also explain mutagenesis studies within a predominantly acidic channel of ionizable residues that runs across C3d and includes the association site. This is the first immunophysical study of the complement system. We hope our study will contribute to the field of design of peptides or small molecules that could modulate the C3d-CR2 association.

References

1. Tsokos, G. C., J. D. Lambris, F. D. Finkelman, E. D. Anastassiou, and C. H. June. 1990. Monovalent ligands of complement receptor 2 inhibit whereas polyvalent ligands enhance anti-Ig-induced human B cell intracytoplasmic free calcium concentration. *J. Immunol. 144:1640.*
2. Fearon, D. T., and J. M. Ahearn. 1990. Complement receptor type 1 (C3/C4b receptor; CD35) and complement receptor type 2 (C3d/Epstein-Barr virus receptor; CD21). *Curr. Top. Microbiol. Immunol. 153:83.*
3. Thyphronitis, G., T. Kinoshita, K. Inoue, J. E. Schweinle, G. C. Tsokos, E. S. Metcalf, F. D. Finkelman, and J. E. Barlow. 1991. Modulation of mouse complement receptor-1 and receptor-2 suppresses antibody responses in vivo. *J. Immunol. 147:224.*

4. Krych, M., J. P. Atkinson, and V. M. Holers. 1992. Complement receptors. *Curr. Opin. Immunol. 4:8*.
5. Tsoukas, C. D., and J. D. Lambris. 1993. Expression of EBV/C3d receptors on T cells: biological significance. *Immunol. Today 14:56*.
6. Carroll, M. C., and M. B. Fischer. 1997. Complement and the immune response. *Curr. Opin. Immunol. 9:64*.
7. Ahearn, J. A., and A. M. Rosengard. 1998. Complement receptors. In *The Human Complement System in Health and Disease*. J. E. Volanakis and M. Frank, eds. Marcel Dekker, New York, p. 167.
8. Carroll, M. C. 1998. The role of complement and complement receptors in induction and regulation of immunity. *Annu. Rev. Immunol. 16:545*.
9. Tolnay, M., and G. C. Tsokos. 1998. Complement receptor 2 in regulation of the immune response. *Clin. Immunol. Immunopathol. 88:123*.
10. Fearon, D. T., and M. C. Carroll. 2000. Regulation of B lymphocyte responses to foreign and self-antigens by the CD19/CD21 complex. *Annu. Rev. Immunol. 18:393*.
11. Barrington, R., M. Zhang, M. Fischer, and M. C. Carroll. 2001. The role of complement in inflammation and adaptive immunity. *Immunol. Rev. 180:5*.
12. Hannan, J., K. Young, G. Szakonyi, M. J. Overduin, S. J. Perkins, X. Chen, and V. M. Holers. 2002. Structure of complement receptor (CR) 2 and CR2–C3d complexes. *Biochem. Soc. Trans. 30:983*.
13. Lowell, C. A., L. B. Klickstein, R. H. Carter, J. A. Mitchell, D. T. Fearon, and J. M. Ahearn. 1989. Mapping of the Epstein-Barr virus and C3dg binding sites to a common domain on complement receptor type 2. *J. Exp. Med. 170:1931*.
14. Carel, J. C., B. L. Myones, B. Frazier, and V. M. Holers. 1990. Structural requirements for C3d,g/Epstein-Barr virus receptor (CR2/CD21) ligand binding, internalization, and viral infection. *J. Biol. Chem. 265:12293*.
15. Molina, H., C. Brenner, S. Jacobi, J. Gorka, J. C. Carel, T. Kinoshita, and V. M. Holers. 1991. Analysis of Epstein-Barr virus-binding sites on complement receptor 2 (CR2/CD21) using human-mouse chimeras and peptides: at least two distinct sites are necessary for ligand-receptor interaction. *J. Biol. Chem. 266:12173*.
16. Molina, H., S. J. Perkins, J. Guthridge, J. Gorka, T. Kinoshita, and V. M. Holers. 1995. Characterization of a complement receptor 2 (CR2, CD21) ligand binding site for C3: an initial model of ligand interaction with two linked short consensus repeat modules. *J. Immunol. 154:5426*.
17. Aubry, J. P., S. Pochon, J. F. Gauchat, A. Nueda-Marin, V. M. Holers, P. Graber, C. Siegfried, and J. Y. Bonnefoy. 1994. CD23 interacts with a new functional extracytoplasmic domain involving *N*-linked oligosaccharides on CD21. *J. Immunol. 152:5806*.
18. Prodinger, W. M., M. G. Schwendinger, J. Schoch, M. Kochle, C. Larcher, and M. P. Dierich. 1998. Characterization of C3dg binding to a recess formed between short consensus repeats 1 and 2 of complement receptor type 2 (CR2; CD21). *J. Immunol. 161:4604*.
19. Szakonyi, G., J. M. Guthridge, D. Li, K. Young, V. M. Holers, and X. S. Chen. 2001. Structure of complement receptor 2 in complex with its C3d ligand. *Science 292:1725*.
20. Guthridge, J. M., J. K. Rakstang, K. A. Young, J. Hinshelwood, M. Aslam, A. Robertson, M. G. Gipson, M. R. Sarrias, W. T. Moore, M. Meagher, et al. 2001. Structural studies in solution of the recombinant N-terminal pair of short consensus/complement repeat domains of complement receptor type 2 (CR2/CD21) and interactions with its ligand C3dg. *Biochemistry 40:5931*.
21. Guthridge, J. M., K. Young, M. G. Gipson, M. R. Sarrias, G. Szakonyi, X. S. Chen, A. Malaspina, E. Donoghue, J. A. James, J. D. Lambris, et al. 2001. Epitope mapping using the x-ray crystallographic structure of complement receptor type 2 (CR2)/CD21: identification of a highly inhibitory monoclonal antibody that directly recognizes the CR2–C3d interface. *J. Immunol. 167:5758*.
22. Prota, A. E., D. R. Sage, T. Stehle, and J. D. Fingeroth. 2002. The crystal structure of human CD21: implications for Epstein-Barr virus and C3d binding. *Proc. Natl. Acad. Sci. USA 99:10641*.
23. Perkins, S. J., H. E. Gilbert, M. Aslam, J. Hannan, V. M. Holers, and T. H. J. Goodship. 2002. Solution structures of complement components by x-ray and neutron scattering and analytical ultracentrifugation. *Biochem. Soc. Trans. 30:996*.
24. Barlow, P. N., D. G. Norman, A. Steinkasserer, T. J. Horne, J. Pearce, P. C. Driscoll, R. B. Sim, and I. D. Campbell. 1992. Solution structure of the fifth repeat of factor H: a second example of the complement control protein module. *Biochemistry 31:3626*.
25. Barlow, P. N., A. Steinkasserer, D. G. Norman, B. Kieffer, A. P. Wiles, R. B. Sim, and I. D. Campbell. 1993. Solution structure of a pair of complement modules by nuclear magnetic resonance. *J. Mol. Biol. 232:268*.
26. Wiles, A. P., G. Shaw, J. Bright, A. Perczel, I. D. Campbell, and P. N. Barlow. 1997. NMR studies of a viral protein that mimics the regulators of complement activation. *J. Mol. Biol. 272:253*.
27. Casasnovas, J. M., M. Larvie, and T. Stehle. 1999. Crystal structure of two CD46 domains reveals an extended measles virus-binding surface. *EMBO J. 18:2911*.
28. Henderson, C. E., K. Bromek, N. P. Mullin, B. O. Smith, D. Uhrin, and P. N. Barlow. 2001. Solution structure and dynamics of the central CCP module pair of a poxvirus complement control protein. *J. Mol. Biol. 307:323*.
29. Murthy, K. H., S. A. Smith, V. K. Ganesh, K. W. Judge, N. Mullin, P. N. Barlow, C. M. Ogata, and G. J. Kotwal. 2001. Crystal structure of a complement control protein that regulates both pathways of complement activation and binds heparan sulfate proteoglycans. *Cell 104:301*.
30. Herbert, A., J. O'Leary, M. Krych-Goldberg, J. P. Atkinson, and P. N. Barlow. 2002. Three-dimensional structure and flexibility of proteins of the RCA family-a progress report. *Biochem. Soc. Trans. 30:990*.
31. Smith, B. O., R. L. Mallin, M. Krych-Goldberg, X. Wang, R. E. Hauhart, K. Bromek, D. Uhrin, J. P. Atkinson, and P. N. Barlow. 2002. Structure of the C3b binding site of CR1 (CD35), the immune adherence receptor. *Cell 108:769*.
32. Smith, S. A., G. Krishnasamy, K. H. Murthy, A. Cooper, K. Bromek, P. N. Barlow, and G. J. Kotwal. 2002. Vaccinia virus complement control protein is monomeric, and retains structural and functional integrity after exposure to adverse conditions. *Biochim. Biophys. Acta 1598:55*.
33. Moore, M. D., R. G. DiScipio, N. R. Cooper, and G. R. Nemerow. 1989. Hydrodynamic, electron microscopic, and ligand-binding analysis of the Epstein-Barr virus/C3dg receptor (CR2). *J. Biol. Chem. 264:20576*.
34. Diefenbach, R. J., and D. E. Isenman. 1995. Mutation of residues in the C3dg region of human complement component C3 corresponding to a proposed binding site for complement receptor type 2 (CR2, CD21) does not abolish binding of iC3b or C3dg to CR2. *J. Immunol. 154:2303*.
35. Clemenza, L., and D. E. Isenman. 2000. Structure-guided identification of C3d residues essential for its binding to complement receptor 2 (CD21). *J. Immunol. 165:3839*.
36. Sarrias, M. R., S. Franchini, G. Canziani, E. Argyropoulos, W. T. Moore, A. Sahu, and J. D. Lambris. 2001. Kinetic analysis of the interactions of complement receptor 2 (CR2, CD21) with its ligands C3d, iC3b, and the EBV glycoprotein gp350/220. *J. Immunol. 167:1490*.
37. Blom, A. M., J. Webb, B. O. Villoutreix, and B. Dahlback. 1999. A cluster of positively charged amino acids in the C4BP α-chain is crucial for C4b binding and factor I cofactor function. *J. Biol. Chem. 274:19237*.
38. Blom, A. M., K. Berggard, J. H. Webb, G. Lindahl, B. O. Villoutreix, and B. Dahlback. 2000. Human C4b-binding protein has overlapping, but not identical, binding sites for C4b and streptococcal M proteins. *J. Immunol. 164:5328*.
39. Nagar, B., R. G. Jones, R. J. Diefenbach, D. E. Isenman, and J. M. Rini. 1998. X-ray crystal structure of C3d: a C3 fragment and ligand for complement receptor 2. *Science 280:1277*.
40. Honig, B., and A. Nicholls. 1995. Classical electrostatics in biology and chemistry. *Science 268:1144*.
41. Yang, A. S., and B. Honig. 1994. Structural origins of pH and ionic-strength effects of protein stability-acid denaturation of sperm whale apomyoglobin. *J. Mol. Biol. 237:602*.
42. Morikis, D., A. H. Elcock, P. A. Jennings, and J. A. McCammon. 2001. Native-state conformational dynamics of GART: a regulatory pH-dependent coil-helix transition examined by electrostatic calculations. *Protein Sci. 10:2363*.
43. Morikis, D., A. H. Elcock, P. A. Jennings, and J. A. McCammon. 2003. The pH dependence of stability of the activation helix and the catalytic site of GART. *Biophys. Chem. 105:279*.
44. Elcock, A. H., D. Sept, and J. A. McCammon. 2001. Computer simulation of protein-protein interactions. *J. Phys. Chem. B. 105:1504*.
45. Froloff, N., A. Windemuth, and B. Honig. 1997. On the calculation of binding free energies using continuum methods: application to MHC class I protein-peptide interactions. *Protein Sci. 6:1293*.
46. Gilson, M. K., T. P. Straatsma, J. A. McCammon, D. R. Ripoll, C. H. Faerman, P. H. Axelsen, I. Silman, and J. L. Sussman. 1994. Open back door in a molecular-dynamics simulation of acetylcholinesterase. *Science 263:1276*.
47. Morikis, D., A. H. Elcock, P. A. Jennings, and J. A. McCammon. 2001b. Proton transfer dynamics of GART: the pH-dependent catalytic mechanism examined by electrostatic calculations. *Protein Sci. 10:2379*.
48. Tanford, C., and J. G. Kirkwood. 1957. Theory of protein titration curves. I. General equations for impenetrable spheres. *J. Am. Chem. Soc. 79:5333*.
49. Tanford, C., and R. Roxby. 1972. Interpretation of protein titration curves: application to lysozyme. *Biochemistry 11:2192*.
50. Bashford, D., and M. Karplus. 1990. pKas of ionizable groups in proteins-atomic detail from a continuum electrostatic model. *Biochemistry 44:10219*.
51. Bashford, D., and M. Karplus. 1991. Multiple-site titration curves of proteins-an analysis of exact and approximate methods for their calculations. *J. Phys. Chem. 95:9556*.
52. Antosiewicz, J., J. A. McCammon, and M. K. Gilson. 1994. Prediction of pH-dependent properties of proteins. *J. Mol. Biol. 238:415*.
53. Antosiewicz, J., J. A. McCammon, and M. K. Gilson. 1996. The determinants of pK_as in proteins. *Biochemistry 35:7819*.
54. Davis, M. E., J. D. Madura, B. A. Luty, and J. A. McCammon. 1991. Electrostatics and difussion of molecules in solution: simulations with the University of Houston Brownian dynamics program. *Comp. Phys. Chem. 62:187*.
55. Madura, J. D., M. E. Davis, M. K. Gilson, R. C. Wade, B. A. Luty, and J. A. McCammon. 1994. Biological applications of electrostatic calculations and Brownian dynamics simulations. *Rev. Comput. Chem. 5:229*.
56. Gilson, M. K. 1993. Multiple-site titration and molecular modelling: two rapid methods for computing energies and forces for ionizable groups in proteins. *Proteins 15:266*.
57. Sitkoff, D., K. A. Sharp, and B. Honig. 1994. Accurate calculation of hydration free energies using macroscopic solvent models. *J. Phys. Chem. 98:1978*.
58. Gilson, M. K., and B. Honig. 1988. Calculation of the total electrostatic energy of a macromolecular system: solvation energies, binding energies, and conformational analysis. *Proteins 4:7*.
59. Gilson, M. K., and B. H. Honig. 1988. Energetics of charge-charge interactions in proteins. [Published erratum appears in *1992 Proteins 12:201*.] *Proteins 3:32*.
60. Davis, M. E., and J. A. McCammon. 1991. Dielectric boundary smoothing in finite difference solutions of the Poisson equation: an approach to improve accuracy and convergence. *J. Comput. Chem. 12:909*.
61. Elcock, A. H., and J. A. McCammon. 1998. Electrostatic contributions to the stability of halophilic proteins. *J. Mol. Biol. 280:731*.

62. Hasted, J. B., D. M. Ritson, and C. H. Collie. 1948. Dielectric properties of aqueous ionic solutions. Part I. *J. Chem. Phys. 16:1*.
63. Berman, H. M., J. Westbrook, Z. Feng, G. Gilliland, T. N. Bhat, H. Weissig, I. N. Shindyalov, and P. E. Bourne. 2000. The Protein Data Bank. *Nucleic Acids Res. 28:235*.
64. Vriend, G. 1990. WHAT IF: a molecular modeling and drug design program. *J. Mol. Graphics 8:52*.
65. Nielsen, J. E., K. V. Andersen, B. Honig, R. W. Hooft, G. Klebe, G. Vriend, and R. C. Wade. 1999. Improving macromolecular electrostatics calculations. *Protein Eng. 12:657*.
66. Hooft, R. W. W., C. Sander, and G. Vriend. 1996. Positioning hydrogen atoms by optimizing hydrogen-bond networks in protein structures. *Proteins 26:363*.
67. Koradi, R., M. Billeter, and K. Wuthrich. 1996. MOLMOL: a program for display and analysis of macromolecular structures. *J. Mol. Graphics 14:51*.
68. Nicholls, A., K. A. Sharp, and B. Honig. 1991. Protein folding and association: insights from the interfacial and thermodynamic properties of hydrocarbons. *Proteins 11:281*.
69. Guex, N., and M. C. Peitsch. 1997. SWISS-MODEL and the Swiss-PdbViewer: an environment for comparative protein modeling. *Electrophoresis 18:2714*.
70. Norman, D. G., P. N. Barlow, M. Baron, A. J. Day, R. B. Sim, and I. D. Campbell. 1991. Three-dimensional structure of a complement control protein module in solution. *J. Mol. Biol. 219:717*.
71. Selzer, T., S. Albeck, and G. Schreiber. 2000. Rational design of faster and tighter binding protein complexes. *Nat. Struct. Biol. 7:537*.
72. Lambris, J. D., V. S. Ganu, S. Hirani, and H. J. Muller-Eberhard. 1985. Mapping of the C3d receptor (CR2)-binding site and a neoantigenic site in the C3d domain of the third component of complement. *Proc. Natl. Acad. Sci. USA 82:4235*.
73. Ullmann, G. M., and E. W. Knapp. 1999. Electrostatic models for computing protonation and redox equilibria in proteins. *Eur. Biophys. J. 28:533*.
74. Sheinerman, F. B., R. Norel, and B. Honig. 2000. Electrostatic aspects of protein-protein interactions. *Curr. Opin. Struct. Biol. 10:153*.
75. Simonson, T. 2001. Macromolecular electrostatics: continuum models and their growing pains. *Curr. Opin. Struct. Biol. 11:243*.
76. Baker, N. A., D. Sept, S. Joseph, M. J. Holst, and J. A. McCammon. 2001. Electrostatics of nanosystems: application to microtubules and the ribosome. *Proc. Natl. Acad. Sci. USA 98:10037*.
77. Elcock, A. H. 2002. Modeling supramolecular assemblages. *Curr. Opin. Struct. Biol. 12:154*.
78. Fogolari, F., A. Brigo, and H. Molinari. 2002. The Poisson-Boltzmann equation for biomolecular electrostatics: a tool for structural biology. *J. Mol. Recognit. 15:377*.
79. Simonson, T. 2003. Electrostatics and dynamics of proteins. *Reports on Progress in Physics 66:737*.
80. Morikis, D., M. Roy, M. G. Newlon, J. D. Scott, and P. A. Jennings. 2002. Electrostatic properties of the structure of the docking and dimerization domain of protein kinase A IIα. *Eur. J. Biochem. 269:2040*.